



Fabrication of Nano-holes and Nano-pillars with Laser Interference Lithography

Erden Ertorer^{ab}, Fartash Vasefi^{c,d}, Jeffrey J.L. Carson^{c,d}, and Silvia Mittler^b

^aBiomedical Engineering Program, Faculty of Engineering, Western University, London, ON, Canada

^bDepartment of Physics and Astronomy, Western University, London, ON, Canada

^cImaging Program, Lawson Health Research Institute, London, ON, Canada

^dMedical Biophysics, Schulich School of Medicine and Dentistry,
Western University, London, ON, Canada

Periodic nanostructures have many applications including optical gratings, bio-sensors, photovoltaics, microfiltration, and controlled surface topographies for cell biological applications. Conventional production methods such as Focused Ion Beam (FIB) or Electron Beam Lithography (EBL) are generally expensive, suffer from low speed, and have limited surface coverage. Alternatively, laser interference lithography (LIL) is a fast and relatively inexpensive method to create periodic nanostructures over large areas. In LIL, interference patterns are created by mixing of two coherent beams, which, in turn, are used to expose a photo-resist layer on a substrate. A Lloyd's mirror interferometer is one method for mixing and consists of a mirror placed perpendicular to the substrate on a rotating stage. An expanded laser beam from an objective lens falls on the Lloyd's mirror in such a way that the direct beam and the reflected beam overlap to create an interference pattern on the substrate. The relationship between the periodicity of the interference pattern (d), the wavelength of the laser (λ), and the angle between the mirror and the beam axis (θ) is given by $d = \lambda/2\sin\theta$. Therefore, periodicity can be easily controlled by varying the angle θ .

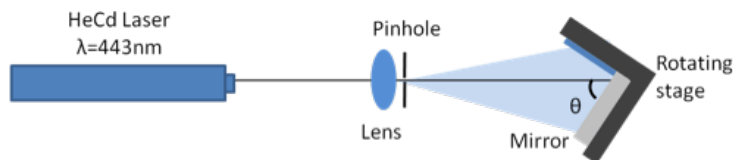


Figure 1 - Illustration of Lloyd's mirror interferometer setup

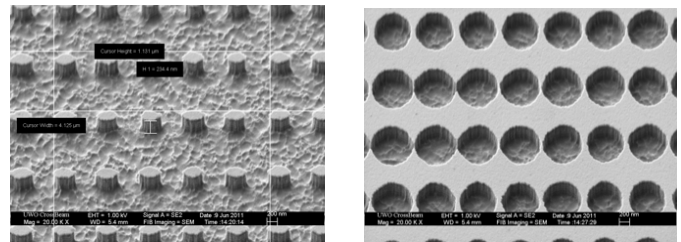
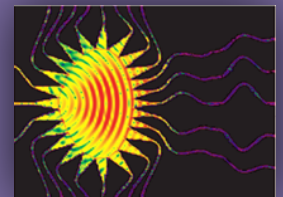


Figure 2 - SEM image of a nano-pillar array (left) and a nano-hole array (right)

We fabricated nano-hole and nano-pillar arrays on a silicon substrate by using LIL (Figure 1). First, 20 nm chromium was deposited on clean silicon substrates with custom e-beam deposition (Hoser, Western Nanofabrication Facility). Substrates were spincoated with Shipley S1805 photoresist at 4000 rpm for 45 seconds resulting in 500 nm film thickness and then they placed on the Lloyd's mirror interferometer at $\theta = 14^\circ$. After the first exposure substrates were rotated 90° and exposed again with $\theta = 10^\circ$, which yielded 2D structures having different periodicities along the x and y axes. The substrates were then developed (MF319 developer, Microchem). Using the photoresist layer as a mask, the substrates were immersed in a chromium etchant to reveal the 2D pattern on the chromium layer. The chromium pattern acted as a secondary mask for the silicon etching process. Then, substrates were placed in the deep reactive ion etching (DRIE) system (Alcatel, 601E, Western Nanofabrication Facility). Remover PG (MicroChem) and chromium etchant were used to remove the photoresist and chromium masks after silicon etching, which resulted in silicon nanopillars or nano-holes.

We characterized the samples with a scanning electron microscope (LEO Zeiss 1540XB FIB/SEM, Western Nanofabrication Facility, Figure 2). Exposures of 25 s ($\theta = 14^\circ$) followed by 19 s ($\theta = 10^\circ$) yielded nano-pillar arrays. Exposures of 22 s ($\theta = 14^\circ$) followed by 15 s ($\theta = 10^\circ$) yielded nano-hole arrays. Sizes of the holes and pillars could be adjusted by fine tuning the exposure time. Depth of the nano-holes and height of the nano-pillars was controlled by the DRIE exposure parameters. The fabricated devices suggest that LIL is a flexible, inexpensive, and fast method for creating periodic nano structures over large areas.





Patterned Ion Beam Implantation of Au and Si via Nanoporous Alumina

Lojan Sivakumaran (Supervisor: Dr. L.V. Goncharova)

Physics and Astronomy, Western University, London ON Canada

Introduction

Porous anodic alumina (PAA) has attracted significant attention as a versatile nanostructure with diverse applications in nanotechnology¹⁻³. The structure consists of a regular array of hexagonal pores arranged in a honeycomb pattern, boasting a high aspect ratio and tunable dimensions. Anodic alumina has piqued both scientific and technological interest as a dielectric film in electrolytic capacitors and as a method for increasing oxidative and abrasion-wear resistance⁴⁻⁵. Currently, PAA has also been identified as a strong candidate for controlling the lateral distribution and size of ion clusters generated via implantation. While there are many methods for the fabrication of nanoparticles on thin films—such as chemical and physical vapour deposition, sol-gel, and beam-induced deposition—ion beam implantation offers many exclusive advantages, such as variability in ion and substrate selection, precise depth-control of the embedded particles, and the highest purity level attainable by any fabrication method.

The ability for PAA to mediate quantum dot formation was investigated on two fronts. Firstly, PAA foils were tested as implantation masks to prevent the overlap of individual ion trajectories into an underlying SiO₂ matrix⁶ (Figure 1). Secondly, since alumina has dielectric properties itself, direct implantation was performed into PAA to generate quantum dots without the need for a secondary substrate. In this case, the pores were suspected to provide the necessary segregation between ion clusters. Regardless of the particular role, film thickness, pore diameter and wall thickness were controlled carefully to prevent the overlap of ion cascades and communication between the nanodots nucleating from each cascade.

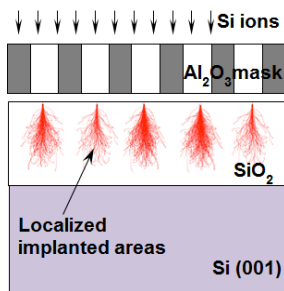


Figure 1. Schematic of ion implantation with the nanoporous alumina mask

Methods - Synthesis of Alumina Substrate and Mask

PAA films were synthesized using a two-step anodization process. First, pure aluminum foils (Alfa Aesar) were annealed for two hours at 350°C to minimize the occurrence of grain-boundaries and to optimize pore organization. Next, a thick aluminum oxide layer was grown on the pure aluminum substrate in 0.3 M oxalic acid at 40V for approximately 16 hours using an electrolytic cell. This initial layer was then removed in phosphoric acid, leaving behind a honeycomb template on the aluminum surface. A second anodization was then performed under the same conditions for either four or ten minutes; the product of the former was designated as an implantation mask, while the latter was fabricated as a confinement matrix. Afterwards, the residual aluminum on both samples was removed with a 4:1 solution of 0.1 M cupric chloride and 20% wt HCl solution for approximately one hour. At this stage, the confinement matrix was complete; however, further processing was required to generate the alumina mask. The barrier layer of the mask was dissolved in a mild etching solution of 5% phosphoric acid for 20 minutes at 30°C in order to open the basal side of the pores, and the product was then transferred onto a silicon dioxide substrate, which acted as the confinement matrix for quantum dot synthesis.

Implantation Protocols

Gold ions were implanted through the PAA mask into the underlying silicon dioxide substrate to visualize and quantify the mask's ability to stop, transmit, and possibly segregate ions. Implantation was done at a

normal incidence with an energy of 700 keV and a dose of 1×10^{15} ions/cm² over an area of 10 cm² (room temperature, 10⁻⁷ Torr) in the Tandem Ion Scattering Facility at Western University. Stopping and Range of Ions in Matter (SRIM) analysis⁸ was performed in order to verify that the depth of implantation did not exceed the thickness of the alumina mask. SEM analysis was performed after implantation to visualize the distribution of implanted gold ions with LEO 1530/1540 SEM (Zeiss, Nanofabrication Faculty, Western University). Finally, Rutherford Backscattering (RBS) analysis was used to determine the degree of blockage by the mask.

An initial investigation of the ability for PAA to act as a confinement matrix for quantum dot synthesis was also performed. Silicon ions were implanted into the thicker PAA film at a 7° angle to the normal with energy of 90 keV and a dose of 1×10^{17} ions/cm² (room temperature, 10⁻⁷ Torr). After ion implantation, masked samples were annealed at 1100°C for 1 hour in N₂ gas to facilitate dot ripening and substrate repair. Morphological changes in the PAA after implantation were monitored with SEM and photoluminescence (PL) measurements were obtained and compared to sapphire SiO₂ and Si-implanted.

Results - Characterization of Alumina Substrate and Mask

Figure 2 shows cross-sectional (a) and plan view (b) field emission scanning electron microscope (SEM) images of the alumina mask. Notable dimensions include an interpore distance of 110±10 nm, a pore diameter of 85±5 nm and a film thickness of approximately 400±30nm. While the PAA prepared by oxidation for ten minutes was considerably thicker (1000±100 nm) than the alumina mask, all other dimensions were similar.

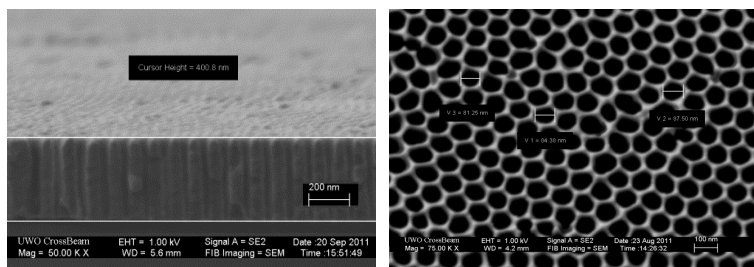


Figure 2. SEM images of porous anodic alumina synthesized at 40 V in 0.3 M oxalic acid for four minutes. (A) Cross sectional view of PAA displaying pore height; wall thickness appears exaggerated due to osmium coatings. (B) Plan view of PAA indicating the pore diameter of 85±5 nm.

Implantation of Gold through Alumina Mask

The Stopping and Range of Ions in Matter (SRIM) analysis⁷ indicated that the implantation profile of ions directly into the mask should not exceed ½ the thickness of the oxide layer. SEM analysis after Au implantation showed the presence of gold clusters on the surface of the mask (Figure 3); this indicated that while the mask was able to intercept the incident ions, the diffusivity of gold in alumina was high enough, even at room temperature, for surface migration. The majority of the gold atoms stopped by the PAA mask formed clusters on the surface approximately 2-12nm in diameter (Figure 2a). Figure 2b shows the effects of implantation from a lateral perspective; while the bottom surface remained fully intact, the implanted surface and the upper walls of the pores were partially deformed. Rutherford Backscattering Spectrometry (RBS) results indicated that the mask was able to stop ion transmission by approximately 75%-90%; only 10-25% of gold ions were implanted into the underlying SiO₂ matrix.

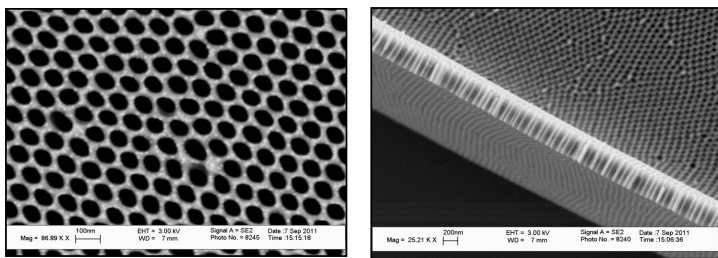


Figure 3. SEM images of PAA implanted with Au ions. (A) Cross-sectional, elevated view of implanted film with a uniform bright layer, indicating Au ion penetration into the mask. (B) Plan view of PAA displaying the segregated Au ions as bright clusters.

Implantation of Silicon into Alumina Confinement Matrix

SEM imaging of the silicon-implanted confinement matrix indicated much greater morphological changes compared to the gold-implanted mask (Figure 4). The cross sectional view provided in Figure 4a emphasizes surface amorphization of the top layer after implantation. A direct comparison between the implanted (amorphized) and non-implanted areas can also be made due to the presence of microscopic debris present pre-implantation (Figure 4b). While amorphization was present, the total PAA film thickness had not been reduced by more than 3%. Interestingly, the geometrical parameters of PAA film, such as thickness of the damaged layer, pore diameter and periodicity, and surface morphology, did not change after annealing at 1100°C.

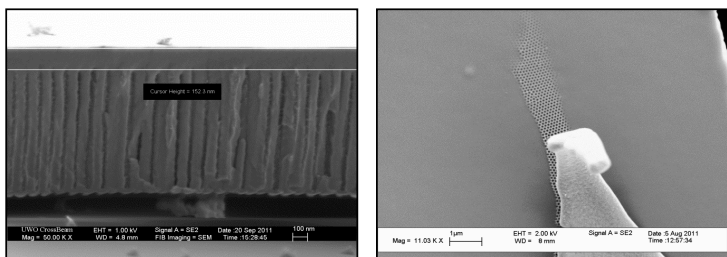


Figure 4. SEM images of PAA implanted with Si ions. (A) Cross sectional view of PAA showing the depth of morphological changes to the surface structure. (B) Plan view of implantation through debris, contrasting the implanted and non-implanted sites.

Photoluminescence spectra of alumina and silicon dioxide, both pre- and post-implantation with silicon, are presented in Figure 5. Photoluminescence of implanted Al_2O_3 shows a broad peak with sharp features at $\sim 700\text{nm}$ that are identical to peaks observed for pure $\alpha\text{-Al}_2\text{O}_3$ (sapphire). A broad signal is present in the 500-700 nm range in the implanted sample that is not seen in the unimplanted Al_2O_3 . A strong peak that is present in the implanted SiO_2 matrix (from 600-900 nm) does not appear in the implanted Al_2O_3 .

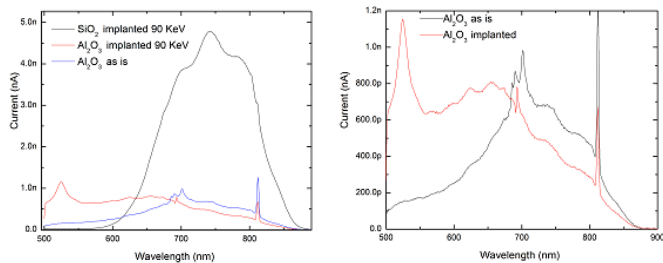


Figure 5. Photoluminescence spectra of unimplanted and implanted Al_2O_3 compared to SiO_2 matrix. (from permission of R. D'Ortenzio)

Discussion

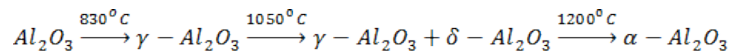
PAA was effectively synthesized as an implantation masks and a confinement matrix. In future experiments, however, addendums/revisions to the protocol may be implemented to modify the PAA's structure and increase its efficacy. For example, parameters such as pore diameter, pore separation and wall

thickness may be adjusted by altering anodization voltage and/or the nature of oxidizing acid (oxalic, sulfuric, or phosphoric etc.)³. These changes (if necessary) will be made hand in hand with the experimental results derived from SEM imaging, RBS analysis and PL spectroscopy in order to optimize Si quantum crystal growth.

SEM and RBS analysis of the normally-implanted Au ions provided evidence that alumina masks were an effective method for intercepting ions at a high energy without surface damage. This indicated that the structure is a strong candidate for segregating implanted semiconductors into an underlying matrix. Future studies will be preformed using silicon and germanium ions to test this hypothesis.

We found that the implantation of Si (10^{17} ions/cm², 90 keV) completely changed the surface morphology of the substrate. The superficial implantation profile suggested a limit on the trajectory of the ions at the given parameters, which was also reported by SRIM data analysis. However, it should be noted that since there was only a maximum $\sim 3\%$ decrease in film thickness, it is unlikely that there were significant sputtering effects at play. These surface effects will be further examined and integrated in future implantation studies in order to generate verifiable quantum dots. PL spectroscopy revealed that the strong peak due to the quantum confinement in Si quantum dots present in implanted SiO_2 matrix did not appear in the implanted Al_2O_3 . This likely indicates that quantum dots were not present in the implanted sample, however future studies will be required to determine why.

While the initial goal of the experiment was to characterize the ability of PAA to generate quantum dots, the necessity of investigating the broad scope effects of implantation on PAA became apparent. It is known that the structure of implanted metal oxides depends upon implantation parameters: dose, energy, ion species, substrate temperature⁸. Temperature, specifically, could play a major role in possible transitions. While the temperatures reported in previous studies were comparable to those in the present investigation (30°C), these temperatures were all measured on the sample holder⁹; local temperature can be significantly higher. The increase in temperature during implantation may enhance defect annihilation, thus favouring the transformation of an amorphous structure to a crystalline one, in the following manner:



Additionally, the long-range effect may also influence structure and morphology throughout the entire thickness of the sample. During implantation, the formation of developed dislocation structures may disorder the structure's crystallinity as the ions propagate in the sample. This effect typically contributes in the transformation of a crystalline structure to an amorphous one. At the same time elastic waves can interact with residual stress in the porous PAA structure, and cause partial rearrangement in local periodicity of the pores.

While initial steps have been taken in the fabrication of quantum dots using PAA, much work is yet to be completed. XRD diffraction studies are underway to identify any α - and δ - Al_2O_3 phases that may be present after implantation and annealing. Further implantation studies will be also performed on PAA samples with varying pore characteristics (pore diameter and inter-pore distance) to control and optimize dot segregation. Finally, subsequent implantation of Si ions and characterization via photoluminescence (PL), high-resolution transmission electron microscopy, and FTIR analysis will ultimately be used determine the efficiency of the segregating procedures in generating Si quantum dots.

References

1. G. D. Sulka, *Nanostructured Materials in Electrochemistry*, Wiley-VCH, Weinheim, 1(2008).
2. H. Masuda, and K. Fukuda, *Science* **268**, 1466 (1995).
3. Y. Lei, and W. K. Chim, *Chem. Mater.* **17**, 580 (2005).
4. F. A. Lowenheim, *Electroplating*, McGraw-Hill Book Company, New York, 452 (1978).
5. S. Wernick, R. Pinner, and P. G. Sheasby, *The Surface Treatment and Finishing of Aluminium and its Alloys*, ASM International, Finishing Publication Ltd., 289 (1987).
6. E.S. Barbagiovanni, L.V. Goncharova, P.J. Simpson, and N. Armstrong, *Mater Res Soc Symp Proc*, 1208 (2010).
7. J.F. Ziegler, J.P. Biersack, U. Littmark, *The Stopping and Range of Ions in Solids*, Pergamon Press, New York, 1985.
8. C.J. McHargue, *Nucl. Instr. and Meth. B* 19-20 (1987) 797.
9. M. Ikeyama, P.Jin, M. Tazawa, *Nucl. Instr. and Meth. B* 148 (1999) 735

Remote Access to the Nanofabrication Facility Scanning Microscope

Over the past two years the staff at the Western Nanofabrication Facility has worked with the Science Studio project to develop a capability to make the Scanning Electron Microscope and X ray detector available to users anywhere in the world. Recently, the final software and hardware components have been installed and preliminary tests look encouraging. The remote service works from any user desktop via the Firefox web browser with support for Java applets. The user sees the same INCA and SmartSEM interface screens for the SEM/EDX as if he/she were physically present (see Figure 1); no delay or “latency” is noticeable as images and spectra are collected. Positioning of the sample in the microscope is done in cooperation with the microscope operator using a Skype connection that is part of the service. All data collected can be uploaded to the user desktop almost as soon as it is acquired. The research session can be followed by any number of members of a scientific team located anywhere in the world.

To use the remote service to Nanofab, existing users need only fill out the simplest of registrations on the Science Studio website (www.sciencestudioproject.com), make arrangements to send samples to the Nanofab and arrange an access time.

Over the next nine months, the Nanofab and the Science Studio would like to involve present users of the Facility who are from outside UWO in tests to improve the service. Those involved in this test program could be compensated by a reduced access fee.

Science Studio is a project sponsored by the CANARIE network and involves remote linkages to science projects in Canada as well as high speed computation of the data collected.

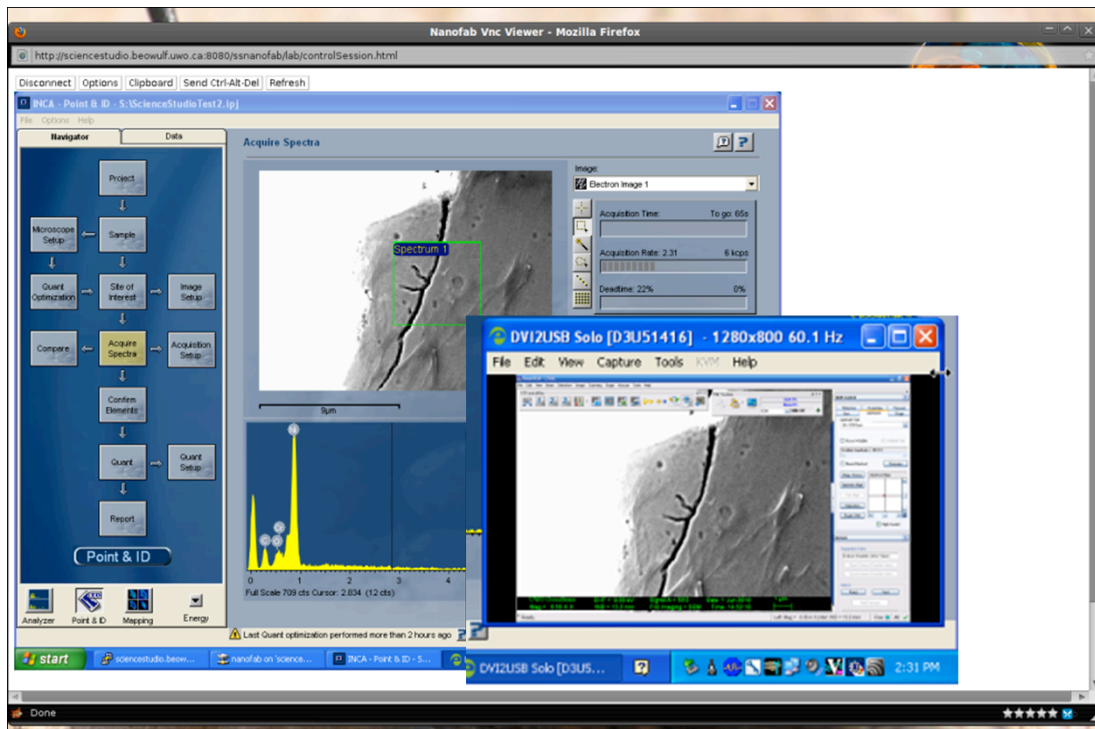


Figure 1 Screenshot of a remote SEM/EDX experiment conducted at the Nanofab using Science Studio software.

The Western Nanofabrication Facility offers an SEM Discount Access Membership for electron microscopy. The academic rate is \$1400 for 60 hours of use and is available for current and new users. The time must be scheduled and used in 3 hour blocks from 1pm to 4pm on our LEO 1530 Field Emission Electron Microscope. For more information or to purchase the SEM Discount Access Membership, please contact Tim Goldhawk.

Western Nanofabrication Facility

Western University
Physics and Astronomy Building Room 14
London, Ontario N6A 3K7

nanofab.uwo.ca



Western
Science

Prof. François Lagugné-Labarthet
Facility Director
flagugne@uwo.ca

Todd Simpson Ph.D.
Senior Research Scientist
tsimpson.uwo.ca

Tim Goldhawk
Laboratory Supervisor
tim.goldhawk@uwo.ca

Dear Nanofabrication graduate students and post-doc, send us a summary of your research project that was done in the Nanofab and receive a \$100 gift card for the Western University bookstore. Your summary could be published in the next NanoWestern newsletter